

Enhancing Cosmological Model Selection with Interpretable Machine Learning

Indira Ocampo,^{1,*} George Alestas,^{1,†} Savvas Nesseris,^{1,‡} and Domenico Sapone^{2,§}

¹*Instituto de Física Teórica UAM-CSIC, Universidad Autónoma de Madrid, Cantoblanco, 28049 Madrid, Spain.*

²*Departamento de Física, FCFM, Universidad de Chile, Santiago, Chile.*

(Dated: June 13, 2024)

We propose a novel approach using neural networks (NNs) to differentiate between cosmological models, especially in the case where they are nested and the additional model parameters are close to zero, making it difficult to discriminate them with traditional approaches. Our method complements Bayesian analyses for cosmological model selection, which heavily depend on the chosen priors and average the unnormalized posterior over potentially large prior volumes. By analyzing simulated realistic data sets of the growth rate of the large scale structure (LSS) of the Universe, based on current galaxy-clustering survey specifications, for the cosmological constant and cold dark matter (Λ CDM) model and the Hu-Sawicki $f(R)$ model, we demonstrate the potential of NNs to enhance the extraction of meaningful information from cosmological LSS data. We find that the NN can successfully distinguish between Λ CDM and the $f(R)$ models, by predicting the correct model with approximately 97% overall accuracy, thus demonstrating that NNs can maximise the potential of current and next generation surveys to probe for deviations from general relativity.

Introduction. The accelerated expansion of the Universe, which the cosmological constant Λ and Cold Dark Matter (Λ CDM) model successfully describes, remains a significant enigma in cosmology due to several tensions that have appeared recently between low redshift and high redshift probes, see for example [1] for a recent review. To account for this phase of accelerated expansion of the Universe, alternative theories of gravity have been proposed, such as various covariant modifications of the Einstein-Hilbert action, from which general relativity (GR) with a cosmological constant can be derived from. The simplest such example is promoting the Lagrangian $R - 2\Lambda$ to a more general function of the Ricci scalar of the form $R + f(R)$ [2–7]. These alternative theories of gravity attempt to change the nature of the gravitational attraction, however they also face challenges in their theoretical justification, as higher-order covariant modifications of GR in general may exhibit ghost-like behavior or the Ostrogradski instability [8]. However, in the simple case of $f(R)$ the latter issue is avoided.

As a result of the intriguing possibility to probe for deviations from GR, over the past two decades a plethora of analyses has been performed, using data from both early Universe physics (e.g., cosmic microwave background (CMB) photons from the Planck [9], ACT [10], and South Pole Telescope [11, 12] experiments) and the distribution of baryonic matter in later times (e.g., BOSS [13–16], DES [17, 18], DESI [19, 20], *Euclid* [21–23]). All these efforts have dramatically decreased the uncertainty in the estimation of cosmological parameters; however, tensions still remain in the parameters even for the favored standard Λ CDM model [24]. Future surveys such as the *Simons Observatory* [25], and the *Vera C. Rubin Observatory*'s Legacy Survey of Space and Time (LSST) [26], aim to further refine the measurements of these parameters. However, the enhanced precision of these experiments demands highly accurate theoretical modeling

and extensive evaluations of the likelihood [27].

Thus, there is a pressing need to develop more intricate astrophysical and cosmological models, incorporating numerous nuisance parameters to properly capture astrophysical phenomena [28–31]. Furthermore, it is essential to test various cosmological models that predict the same or very similar expansion histories. Typically, such comparisons rely on a likelihood function and calculations of Bayes factors [32] to determine the preferred model. However, this approach has its limitations, mainly due to the very high computational cost, especially when dozens or more nuisance parameters are taken into account (as is the case of the Planck likelihood [33]), but also due to the dependency on ad-hoc priors and the averaging of the unnormalized posterior over prior volumes, which can affect each model differently. Moreover, the Bayesian comparison does not outright reject models, but rather evaluates which one is comparatively more supported by the data, based on the Jeffreys' scale [34].

To address the aforementioned issues, we turn to machine learning (ML), which has become a cornerstone in the landscape of artificial intelligence (AI) techniques. Its main advantage is in extracting patterns, insights, and knowledge from vast amounts of data without explicit instructions, and can adjust and improve autonomously.

In astronomy, ML has recently seen a plethora of practical applications facilitating the automation of the identification of celestial objects and specific patterns of the sources [35–47], given the volume of data from ongoing surveys, manual analysis has become challenging. Also, in high-energy experiments like the Large Hadron Collider, the volume of data produced is enormous. ML can facilitate the creation of efficient triggers by filtering out irrelevant data, pin-pointing significant events, and providing insights that manual analyses might miss [48–50].

Given the aforementioned challenges in standard analyses, but also the unique advantages of ML, in this work

we propose a novel approach to enhance model selection for discriminating between different cosmological models. Specifically, we explore neural networks (NNs) as a tool that can complement traditional Bayesian analysis, offering a new perspective in extracting meaningful information, especially in cases where there are degeneracies in the parameter space, several nuisance parameters or ad-hoc chosen priors, all of which may affect traditional analyses. Furthermore, as ML techniques are gaining a lot of attention and being exploited in almost every field of study nowadays, there is a need to unveil its complexity and understand its decision making process. Thus, in the present work we also study the NN interpretability, so as to understand which are the relevant features that have a more significant impact in the classification. In particular, we perform this analysis using LIME [51].

To demonstrate the advantage of our approach, we performed analyses using realistic, simulated data sets based on a Stage-IV LSS survey, for two distinct cosmological models: the Λ CDM model and a specific class of the Hu-Sawicki $f(R)$ model [4, 52], where the latter replicates the Λ CDM background expansion precisely, while it differs in the growth of matter distribution, thus guaranteeing that the only information used comes from the growth of structures in our Universe.

Our study specifically targets a DESI-like survey to assess these models, which is particularly timely as the recent DESI DR1 data release and the resulting cosmological constraints [19], showed exciting hints for a possible time evolution of the dark energy equation of state parameter $w(z)$, which in the Λ CDM takes the value $w(z) = -1$. This possible redshift evolution of $w(z)$ seen by DESI, further motivates our work as it could hint to either the presence of a scalar field [53–55] or some deviation from GR [56]. However, special care should be taken when perturbations in the dark sector are considered [57].

Setting the stage. In order to keep the analysis simple, in this work we will consider two models: the Λ CDM model and the Hu-Sawicki $f(R)$ model (HS), described by the action [4]

$$S = \int d^4x \sqrt{-g} \left\{ \frac{1}{2\kappa^2} [R + f(R)] + \mathcal{L}_m \right\}, \quad (1)$$

where \mathcal{L}_m is the matter Lagrangian, $\kappa^2 = \frac{8\pi G_N}{c^4}$, and the $f(R)$ function for $|f_R| \ll 1$ is approximately equal to

$$f(R) = -6 \Omega_{\text{DE},0} \frac{H_0^2}{c^2} + |f_{R0}| \frac{\bar{R}_0^2}{R} + \dots, \quad (2)$$

where $f_{R0} = df(R)/dR|_{z=0}$. For values of $|f_{R0}| \ll 1$, the background expansion history is well approximated by Λ CDM [58], and here we use $|f_{R0}| = 5 \times 10^{-6}$, which is in agreement with observations and it also allows us to compare the results with Ref. [59].

Then, as the background expansion is similar to that of the Λ CDM model, we turn to the matter density per-

turbations of the large scale structure (LSS) of the Universe, and in particular the growth-rate of the matter density contrast $\delta_m \equiv \delta\rho_m/\rho_m$. The growth-rate is then defined as $f \equiv d \ln \Delta_m / d \ln a$, where a is the scale factor that describes the expansion of the Universe in an Friedmann–Lemaître–Robertson–Walker (FLRW) geometry and $\Delta_m(a) \equiv \delta_m(a)/\delta_m(a=1)$ is the normalized to today growth.

However, what is actually measurable by LSS and galaxy-clustering spectroscopic surveys is instead the quantity $f\sigma_8(a) \equiv f(a) \sigma_8(a) = \sigma_{8,0} a \Delta'_m(a)$, where $\sigma_8(a) = \sigma_{8,0} \Delta_m(a)$ is the redshift-dependent root mean square (RMS) fluctuations of the linear density field at $R = 8 h^{-1} \text{Mpc}$ and $\sigma_{8,0}$ is its present value. Then, $f\sigma_8(a)$ can be measured directly via the monopole to the quadrupole ratio of the redshift-space power spectrum, that depends on the parameter $\beta = f/b$, where b is the galaxy bias, thus making $f\sigma_8(a)$ bias-free, as the bias cancels out from the expression. Finally, $f\sigma_8$ was shown in Ref. [60] to be an effective discriminator of dark energy (DE) and modified gravity (MG) models, making it ideal for our analysis.

Finally, we also need to model the three-dimensional matter power spectrum, which is a measure of the variance of the density contrast, and is the Fourier transform of the 2-point correlation function [61]. Then, the observed galaxy power spectrum is modeled as in [62]:

$$P_{\text{obs}}(k, \mu; z) = \frac{H(z) D_{A,r}(z)}{H_r(z) D_A(z)} [b(z)\sigma_8(z) + f(z)\sigma_8(z)\mu^2]^2 \times \frac{P_{\text{nl}}(k, \mu; z)}{\sigma_8^2(z)} e^{-k^2 \mu^2 \sigma_r^2} + P_s(z), \quad (3)$$

where μ is the angle of the wave-vector k with respect to the line of sight, and the P_{nl} is the matter power spectrum with non-linear corrections damping the BAO signal, see [59, 63]; the first term is the Alcock-Paczynski effect, which takes into account the change on volume via the Hubble parameter $H(z)$ and the angular diameter distance $D_A(z)$, while $P_s(z)$ is the shot-noise term. The galaxy matter power spectrum is further modulated [62] by an error in the redshift measurement $\sigma_r^2 = c \delta z / H(z)$ with $\delta z = 0.0005(1+z)$. The linear matter power spectrum for the models used in this work has been obtained using MGCAMB [64–67].

In order to simulate the data, we will assume a DESI-like survey, covering $14\,000 \text{ deg}^2$, whose targets are: Bright Galaxies (BGs) at low redshifts $z < 0.4$, Luminous Red Galaxies (LRGs) at redshifts $0.4 < z < 1.1$, Emission Line Galaxies (ELGs) at redshifts $0.6 < z < 1.6$, and quasars at $0.9 < z < 2.1$, [20, 68]. In this work, we use only BGs to cover low redshifts and ELG to cover high redshifts having in total 16 redshift bins.

To evaluate the covariance matrix we use the Fisher matrix approach, the cosmological parameters are the Hubble parameter $H(z)$, $D_A(z)$, $f\sigma_8(z)$, $b\sigma_8(z)$, and

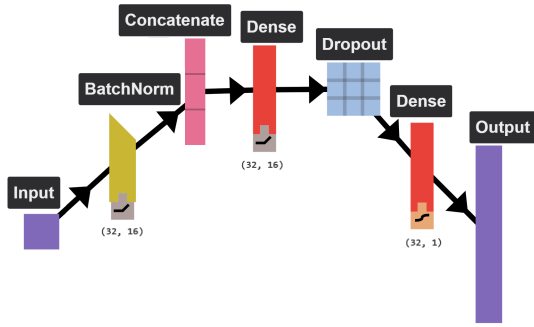


FIG. 1: Visualization of the architecture of our NN, where we show how we implemented feature normalization with a ReLU activation function, followed by a concatenation layer. After that, the data passes through a fully connected layer also with a ReLU activation and a dropout layer, with a `dropout_rate=0.2`, to finally go through another fully connected layer with a sigmoid activation function and take a decision about the particular class.

$P_s(z)$. While the shape parameters $\omega_{m,0} = \Omega_{m,0}h^2$, h , $\omega_{b,0} = \Omega_{b,0}h^2$, n_s are kept fixed. The latter implies setting priors from CMB experiments [69]. The specific Fisher matrix will have dimension 16 bins \times 5 parameters per bin = 80 parameters. The bias factor and the shot-noise are considered nuisance parameters, to be marginalised over. Regarding the $f\sigma_8(z)$, in any modified theory model or if dark energy perturbations are present, the growth rate depends on the scale k , see [70]. In this work, in order to constrain $f\sigma_8(z)$, we relaxed this assumption and took the value of the growth rate at $k = 0.01 \text{ Mpc}^{-1}$, since the dependence across the entire k range is less than 0.1%.

The final covariance matrix for DESI-like specifications is obtained from the marginalization of the Fisher matrix. As the dependence of the covariance matrix on the cosmology is weak, especially as the $f(R)$ model is close to Λ CDM, we use the same covariance for both models, based on a fiducial cosmology of $\Omega_{m,0} = 0.32$, $\Omega_{b,0} = 0.05$, $h = 0.67$, $n_s = 0.96$, and $\sigma_{8,0} = 0.85$.

Simulated data. In order to test deviations from Λ CDM with our methodology, we simulated DESI-like datasets for $f\sigma_8$ measurements reflecting both cosmological models: Λ CDM and HS. Using the specifications, as discussed earlier, we generate mock datasets using grids within the following intervals: $\Omega_{m,0} \in [0.2, 0.4]$ and $\sigma_{8,0} \in [0.7, 0.9]$ for Λ CDM, while for the HS model, we vary the parameters in the range $\Omega_{m,0} \in [0.2, 0.4]$, $\sigma_{8,0} \in [0.7, 0.9]$ and $fR_0 \in [10^{-6}, 5 \times 10^{-6}]$, where these values were chosen so that they are in agreement with current observational constraints for the two models.

NN architecture. In summary, the architecture implemented, is the one shown in Fig. 1 created with

ENNUI.¹ The input data are $f\sigma_8$ values for a DESI-like survey with 16 z -bins, where we took into account the uncertainties from the Fisher matrix approach. We first implemented a feature normalization layer, with a ReLU activation function [71], where we set the `batch_size` to 32 (for each one of the 16 features). After normalization, we concatenated the features and passed the full data set through a fully connected layer, also with a ReLU activation function. Then, we applied a dropout layer, which is a regularization technique for preventing overfitting [72], with a dropout rate of 0.2, and finally the last fully connected layer with a sigmoid activation for the classification task: HS (class 1) or Λ CDM (class 0). We also applied an early stopping callback [73] to prevent overfitting, for this we set the “patience” (the number of epochs in which the accuracy and loss do not change significantly) to 50 training epochs, and found that our model reached a high accuracy and low loss in 1400 epochs, see Fig. 2. Our model was compiled with a nadam optimizer [74], a binary cross entropy loss function and a learning rate of 0.001.

Results. The full dataset has 5000 $f\sigma_8$ samples (50% HS and 50% Λ CDM), that we split as 70% for training + validation and 30% for testing. In Fig. 2 we show the accuracy and loss with respect to the number of epochs optimized by the early stopping callback. We observe that in both cases the NN has demonstrated well-converged loss and accuracy metrics. Specifically, the training loss decreased smoothly from 0.7 to about 0.1, while the validation loss similarly decreased from 0.68 to 0.04, showing minimal fluctuations. The training accuracy improved from 52% to 97%, with the validation accuracy closely following, improving from 58% to 99%. The alignment between training and validation metrics indicates minimal overfitting, and the final plateau in both loss and accuracy suggests that the model has converged to an optimal state. Finally, in Fig. 3 we show the confusion matrix, where we notice that the NN performs very well, as it can correctly identify the Λ CDM model 100% of the time and the HS model $\sim 95\%$ of the time, while offering false positives only in the rest $\sim 5\%$, these results in an overall accuracy rate of 97.5% for a correct prediction.

Robustness of the NNs. We have performed several tests in order to test the robustness of our pipeline. First, we examined the effect of dataset size on the performance of the NN, as shown in Fig. 4. The results indicate that the correct predictions saturates after a few thousand realizations. Considering that the running time of the NN scales approximately linearly with the number of mock datasets, we chose a dataset size of 5000 realizations. This choice represents a compromise between running time and the accuracy of the NN.

¹ <https://github.com/martinjm97/ENNUI.git>

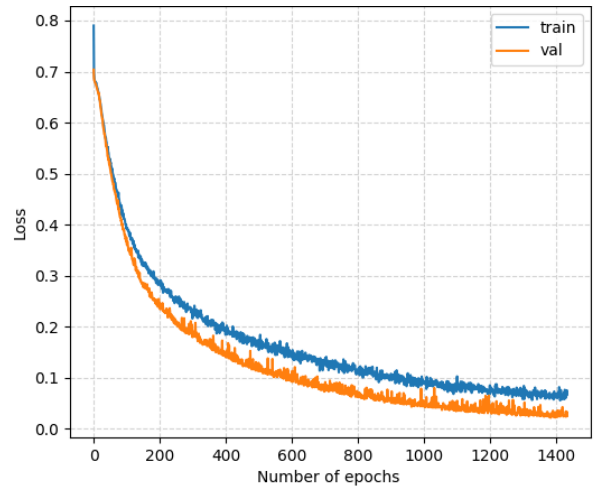
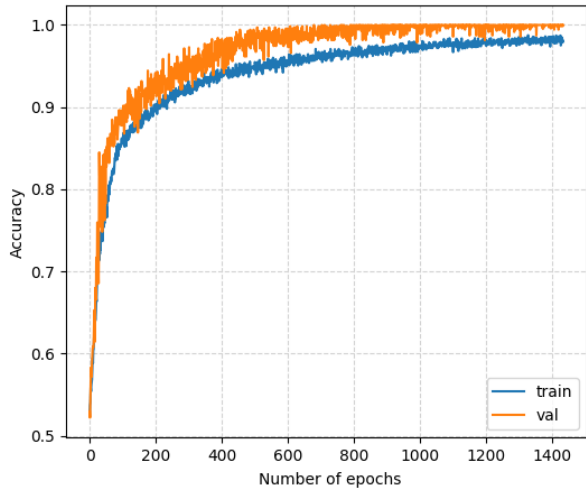


FIG. 2: The accuracy and loss curves of the model (left and right panels respectively), with respect to the number of training epochs, for the training (blue line) and validation (orange line).

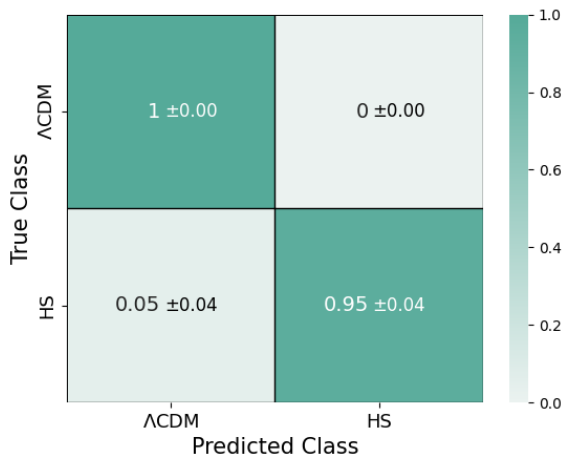


FIG. 3: The confusion matrix of the NN. As can be seen, the NN performs exceptionally well in discriminating the two models, predicting Λ CDM and the HS models with 100% and 95% accuracy, respectively. Note that the probabilities sum to unity horizontally.

We also investigated the NN’s performance using simulated data sets based on different covariance matrices. One matrix encapsulated the inherent variations within the noise profile of the Λ CDM model, while the other represented the noise profile associated with the $f(R)$ model. We found that the NN can also accurately discriminate 100% both models when utilizing different covariance matrices, albeit at the cost of adding some biases in the results. The reason for this is that the NN in this case also learns to discriminate the covariance matrix, i.e. if it belongs to Λ CDM or $f(R)$, via the noise distribution of the $f\sigma_8$ data.

NN interpretability. In order to identify which fea-

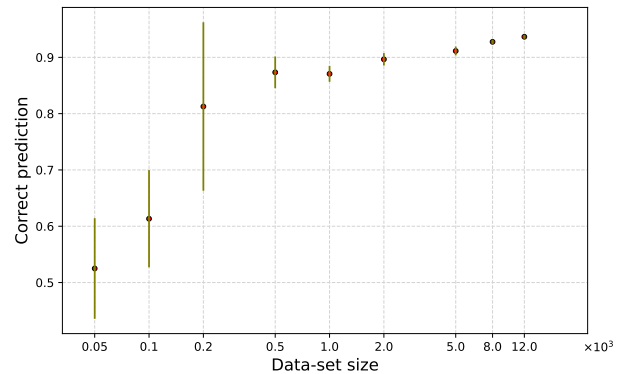


FIG. 4: Correct prediction performed by the Neural Network with respect to the number of dataset samples in semi-log scale, and the corresponding errors.

tures of the data help the NN discriminate so well between the two models, we next investigate the *NN interpretability* [75]. The first test to identify the most relevant features in the NN’s decision-making process was carried out by training and testing using only the first eight and last eight $f\sigma_8$ values. We found that the performance is predominantly influenced by the first eight features. An interesting approach for this interpretability task, is the one implemented by LIME, which stands for Local Interpretable Model-agnostic Explanations. The local interpretability procedure is a less complicated task to tackle compared to the global one, therefore this approach aims to understand the model’s decision-making process by generating nearby data points through random perturbations of the features from a given data-point and then analyzing how these changes affect the model’s predictions. Then, it learns locally weighted lin-

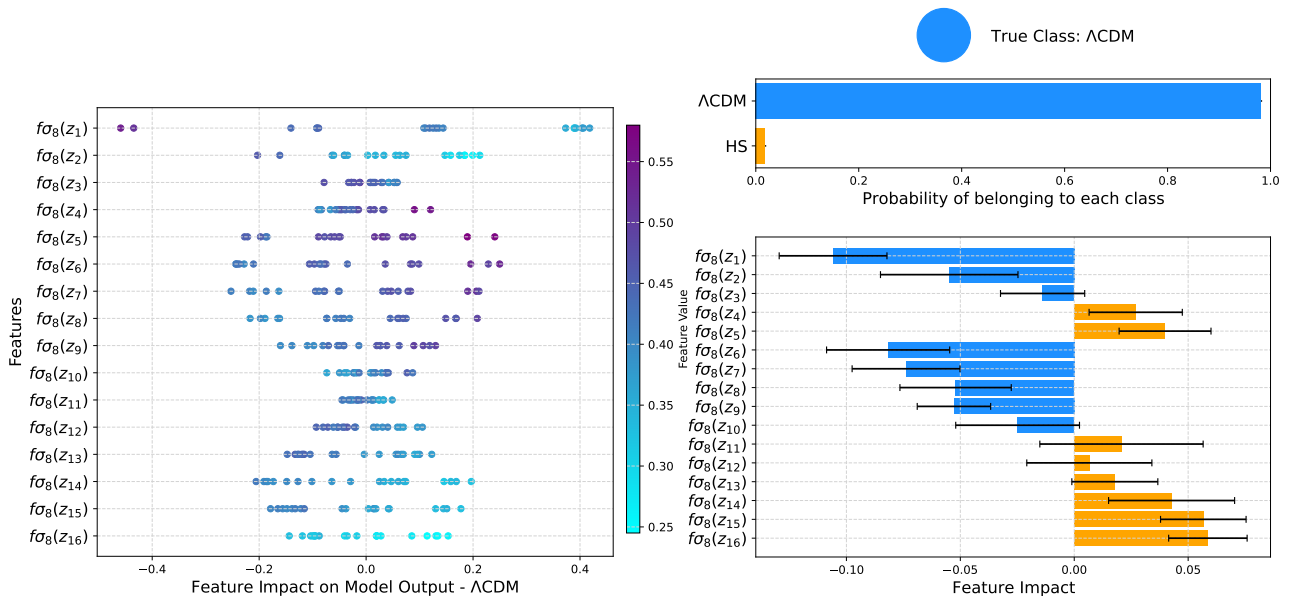


FIG. 5: Left: The individual impact from each random perturbation for each feature on whether it is classified as one of the two models: Λ CDM (negative values on x-axis) or HS (positive values on the x-axis). Right: A particular example of one particular data sample of the test set, shown at each redshift bin. In this case, the true model is Λ CDM.

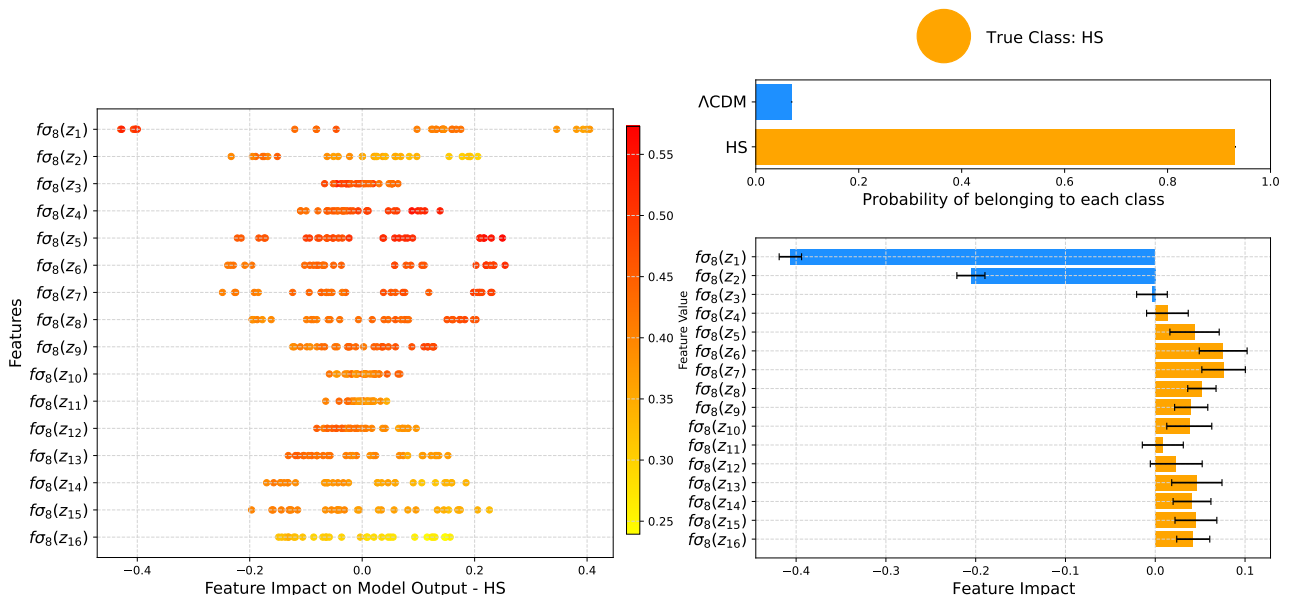


FIG. 6: As in Fig. 5, but the true class is the HS model.

ear models on this neighborhood data to explain each of the classes in an interpretable way [76, 77].

In Figs. 5 and 6 we show the feature impact on the model output for our NN. First we picked a data sample from the test set (that was correctly classified), belonging to the Λ CDM and then one to the HS classes respectively. LIME calculates the individual probability of each feature to belong to a determined class, given that it has a particular value, and then obtains an overall probability of belonging to HS or Λ CDM. In Fig. 5, the overall probability of belonging to class Λ CDM is around 0.99, and the most relevant features that have an impact are found to

be $f\sigma_8(z_1)$, $f\sigma_8(z_6)$ and $f\sigma_8(z_7)$, whereas in Fig. 6, the overall probability of belonging to class HS is around 0.9, and the most relevant features that have an impact are found to be $f\sigma_8(z_6)$, $f\sigma_8(z_7)$ and $f\sigma_8(z_8)$. The positive x-axis in both figures illustrates the local probability of belonging to class HS, and the negative to class Λ CDM.

Also, in both cases on the left panel we show the individual impact from each random perturbation for each feature on whether it is classified locally, as Λ CDM (negative values on the x-axis) or HS (positive values on the x-axis). The samples in Fig. 5 were classified overall as Λ CDM and the ones in Fig. 6 as HS. The $f\sigma_8$ values are

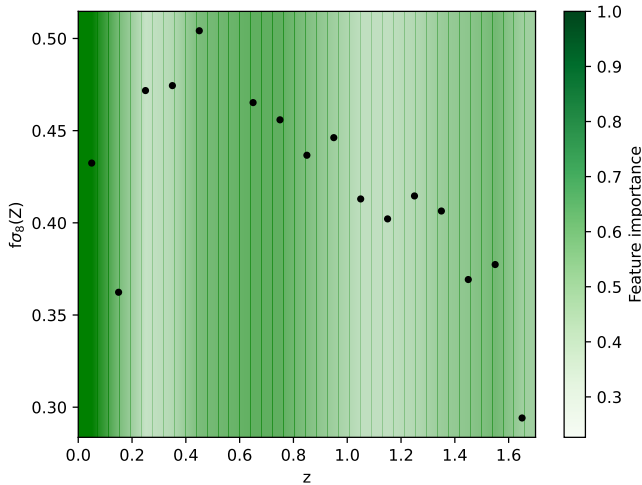


FIG. 7: One realization of $f\sigma_8$ data, as a function of the redshift z . The color shading corresponds to the feature importance of each redshift bin (a darker shade implies stronger feature importance), according to the tests from LIME.

also displayed as a heat map, bearing in mind that this analysis was performed for 50 samples of the test set. We can see that in both cases, the overall most important features seem to be the first $f\sigma_8(z_1)$, then three in the middle $f\sigma_8(z_5)$, $f\sigma_8(z_6)$, $f\sigma_8(z_7)$, $f\sigma_8(z_8)$ and two at the end $f\sigma_8(z_{14})$, $f\sigma_8(z_{15})$.

Finally, in Fig. 7 we show the values of one realization of $f\sigma_8$ data with respect to the redshift z . The color shading corresponds to the feature importance of each redshift bin (light to dark green implying low to high importance), according to the tests from LIME discussed earlier. As can be seen, the most important redshift bins are at low ($z < 0.2$), albeit with mid ($0.5 < z < 0.8$) and high ($z > 1.4$) redshifts also carrying strong weight (importance ~ 0.5). On the other hand, the intermediate redshifts ($0.2 < z < 0.5$) and $0.8 < z < 1.4$) have particularly low feature importance (below 0.3). This behavior is observationally correct, as the largest differences in the growth rate between the Λ CDM and MG models occur at low redshift. The impact at intermediate redshifts ($z \sim 0.7$) is also clear because this is when the effective DE begins to dominate, and it is where the largest variation, hence the derivative, in the growth factor is observed.

Conclusions. In this work we proposed a NN pipeline that can successfully discriminate between the standard cosmological constant Λ CDM model, which is based on GR, and the most commonly used extension of GR based on the popular HS $f(R)$ model, using LSS growth rate data. While the latter model is still viable, i.e. has not been ruled out yet, the best-fit is so close to Λ CDM that traditional analyses, using galaxy-clustering data, cannot discriminate the two models apart.

Creating an optimized pipeline to do this is a major

goal in light of current surveys, especially in light of the fact that traditional model selection methods, such as Bayesian analyses via the evidence, of course naturally penalize models with more parameters. In this sense, our analysis and pipeline is complementary to the traditional approaches, especially in the case we mention in this work, where due to degeneracies in the data and the fact the extra parameter of the model is close to zero, it is difficult for the traditional analyses to discriminate the two models. In our case, our pipeline performs well in discriminating the two models, to approximately 97%, due to the fact that the NN has more information during the training part compared to the standard analyses which only see one realization at the time. This can be seen particularly clearly in Fig. 4, where we vary the number of mocks used by the NN. When the number of mocks is low, e.g. ~ 50 , the accuracy is as low as 50%, i.e. random change and the NN cannot discriminate the models, but then it saturates over 90% for a few thousand mocks.

Our work focused exclusively on the galaxy-clustering $f\sigma_8$ data as a proof of concept, so as to establish the method and demonstrate its strengths. However, our pipeline can easily be extended to use directly the multipoles of the redshift-space power spectrum and other related observables. Furthermore, we demonstrated the robustness of our approach by studying several aspects, such as the number of training samples, different covariance matrices for the creation of the mock data, but more importantly we also focused on the interpretability of the results, where we identified the aspects of the data that particularly help the NN discriminate the two models.

To our knowledge such a combination of observables used to test directly GR and a related NN pipeline has not been considered before in the literature, while the much simpler task of using NNs to speed up numerical calculations of the evidence is now more common, see for example [78, 79]. Also, the potential to extend our pipeline is significant, especially when used with current LSS surveys and their observables, as it can help discriminate models which are otherwise difficult to tell apart using traditional methods, thus opening a new avenue to probe for deviations of GR with current and next generation surveys.

Code availability. The numerical codes will be made publicly available in GitHub² upon publication of the paper.

Acknowledgements. We would like to thank G. Cañas, S. Casas, and V. Pettorino for useful discussions. IO thanks ESTEC/ESA for the warm hospitality during the execution of this project, and for support from the ESA

² https://github.com/IndiraOcampo/NN-HS_vs_LCDM

Archival Research Visitor Programme. IO, GA and SN acknowledge support from the research project PID2021-123012NB-C43 and the Spanish Research Agency (Agencia Estatal de Investigación) through the Grant IFT Centro de Excelencia Severo Ochoa No CEX2020-001007-S, funded by MCIN/AEI/10.13039/501100011033. GA's and research is supported by the Spanish Attraction de Talento contract no. 2019-T1/TIC-13177 granted by the Comunidad de Madrid. IO is also supported by the fellowship LCF/BQ/DI22/11940033 from "la Caixa" Foundation (ID 100010434). DS acknowledges financial support from the Fondecyt Regular project number 1200171.

* Electronic address: indira.ocampo@csic.es

† Electronic address: g.alestas@csic.es

‡ Electronic address: savvas.nesseris@csic.es

§ Electronic address: domenico.sapone@uchile.cl

- [1] L. Perivolaropoulos and F. Skara, *New Astron. Rev.* **95**, 101659 (2022), 2105.05208.
- [2] H. A. Buchdahl, *Mon. Not. Roy. Astron. Soc.* **150**, 1 (1970).
- [3] A. A. Starobinsky, *Phys. Lett. B* **91**, 99 (1980).
- [4] W. Hu and I. Sawicki, *Phys. Rev. D* **76**, 064004 (2007), 0705.1158.
- [5] A. De Felice and S. Tsujikawa, *Living Rev. Rel.* **13**, 3 (2010), 1002.4928.
- [6] T. P. Sotiriou and V. Faraoni, *Rev. Mod. Phys.* **82**, 451 (2010), 0805.1726.
- [7] S. Capozziello and M. De Laurentis, *Phys. Rept.* **509**, 167 (2011), 1108.6266.
- [8] R. P. Woodard, *Lect. Notes Phys.* **720**, 403 (2007), [astro-ph/0601672](https://arxiv.org/abs/astro-ph/0601672).
- [9] N. Planck Collaboration: Aghanim, Y. Akrami, M. Ashdown, J. Aumont, C. Baccigalupi, M. Ballardini, A. J. Banday, R. B. Barreiro, N. Bartolo, S. Basak, et al., *A&A* **641**, A6 (2020), 1807.06209.
- [10] S. Aiola et al. (ACT), *JCAP* **12**, 047 (2020), 2007.07288.
- [11] L. E. Bleem et al. (SPT), *Astrophys. J. Suppl.* **216**, 27 (2015), 1409.0850.
- [12] S. Bocquet et al. (SPT), *Astrophys. J.* **878**, 55 (2019), 1812.01679.
- [13] S. Alam et al. (BOSS), *Mon. Not. Roy. Astron. Soc.* **470**, 2617 (2017), 1607.03155.
- [14] S. Alam, M. Aubert, S. Avila, C. Balland, J. E. Bautista, M. A. Bershadsky, D. Bizyaev, M. R. Blanton, A. S. Bolton, J. Bovy, et al., *Phys. Rev. D* **103**, 083533 (2021), 2007.08991.
- [15] T. Delubac, J. E. Bautista, N. G. Busca, J. Rich, D. Kirkby, S. Bailey, A. Font-Ribera, A. Slosar, K.-G. Lee, M. M. Pieri, et al., *A&A* **574**, A59 (2015), 1404.1801.
- [16] L. Anderson, É. Aubourg, S. Bailey, F. Beutler, V. Bhardwaj, M. Blanton, A. S. Bolton, J. Brinkmann, J. R. Brownstein, A. Burden, et al., *MNRAS* **441**, 24 (2014), 1312.4877.
- [17] T. M. C. Abbott et al. (DES), *Phys. Rev. D* **105**, 023520 (2022), 2105.13549.
- [18] T. M. C. Abbott et al. (DES) (2021), 2107.04646.
- [19] A. G. Adame et al. (DESI) (2024), 2404.03002.
- [20] G. Adame et al. (DESI) (2023), 2306.06307.
- [21] R. Laureijs et al. (EUCLID) (2011), 1110.3193.
- [22] R. Scaramella et al. (Euclid), *Astron. Astrophys.* **662**, A112 (2022), 2108.01201.
- [23] J. A. A. Barroso et al. (Euclid) (2024), 2405.13491.
- [24] E. Abdalla et al., *JHEAp* **34**, 49 (2022), 2203.06142.
- [25] P. Ade et al. (Simons Observatory), *JCAP* **02**, 056 (2019), 1808.07445.
- [26] R. Mandelbaum et al. (LSST Dark Energy Science) (2018), 1809.01669.
- [27] A. Cole, B. K. Miller, S. J. Witte, M. X. Cai, M. W. Grootes, F. Nattino, and C. Weniger, *JCAP* **09**, 004 (2022), 2111.08030.
- [28] M. Martinelli et al. (Euclid), *Astron. Astrophys.* **649**, A100 (2021), 2010.12382.
- [29] A. Pezzotta et al. (Euclid) (2023), 2312.00679.
- [30] A. Bault et al. (2024), 2402.18009.
- [31] S.-F. Chen et al. (2024), 2402.14070.
- [32] R. E. Kass and A. E. Raftery, *J. Am. Statist. Assoc.* **90**, 773 (1995).
- [33] N. Aghanim et al. (Planck), *Astron. Astrophys.* **641**, A5 (2020), 1907.12875.
- [34] H. Jeffreys, *The Theory of Probability*, Oxford Classic Texts in the Physical Sciences (OUP Oxford, 1998), ISBN 9780191589676.
- [35] K. Voggel et al. (Euclid) (2024), 2405.14015.
- [36] M. S. Cagliari et al. (Euclid) (2024), 2403.08726.
- [37] B. Aussel et al. (Euclid) (2024), 2402.10187.
- [38] T. Signor et al. (Euclid), *Astron. Astrophys.* **685**, A127 (2024), 2402.04800.
- [39] M. Pöntinen et al. (Euclid), *Astron. Astrophys.* **679**, A135 (2023), 2310.03845.
- [40] L. Leuzzi et al. (Euclid), *Astron. Astrophys.* **681**, A68 (2024), 2307.08736.
- [41] A. Humphrey et al. (Euclid), *Astron. Astrophys.* **671**, A99 (2023), 2209.13074.
- [42] P. O. Baqui et al., *Astron. Astrophys.* **645**, A87 (2021), 2007.07622.
- [43] V. Bonjean, N. Aghanim, P. Salomé, A. Beelen, M. Douspis, and E. Soubrié, *Astron. Astrophys.* **622**, A137 (2019), 1901.01932.
- [44] A. Mitra, B. Shukirgaliyev, Y. S. Abylkairov, and E. Abdikamalov (2022), 2209.14542.
- [45] P. D. Aleo et al. (Young Supernova Experiment), *Astrophys. J. Suppl.* **266**, 9 (2023), 2211.07128.
- [46] M. Vincenzi et al. (DES), *Mon. Not. Roy. Astron. Soc.* **518**, 1106 (2023), 2111.10382.
- [47] A. Möller et al. (DES), *Mon. Not. Roy. Astron. Soc.* **514**, 5159 (2022), 2201.11142.
- [48] A. J. Larkoski, I. Moulton, and B. Nachman, *Phys. Rept.* **841**, 1 (2020), 1709.04464.
- [49] D. Guest, K. Cranmer, and D. Whiteson, *Ann. Rev. Nucl. Part. Sci.* **68**, 161 (2018), 1806.11484.
- [50] G. Kasieczka, T. Plehn, M. Russell, and T. Schell, *JHEP* **05**, 006 (2017), 1701.08784.
- [51] M. Tulio Ribeiro, S. Singh, and C. Guestrin, *arXiv e-prints arXiv:1602.04938* (2016), 1602.04938.
- [52] W. Hu and I. Sawicki, *Phys. Rev. D* **76**, 104043 (2007), 0708.1190.
- [53] Y. Tada and T. Terada (2024), 2404.05722.
- [54] K. V. Berghaus, J. A. Kable, and V. Miranda (2024), 2404.14341.
- [55] O. F. Ramadan, J. Sakstein, and D. Rubin (2024), 2405.18747.

- [56] M. Kunz and D. Sapone, *Phys. Rev. Lett.* **98**, 121301 (2007), astro-ph/0612452.
- [57] M. Kunz and D. Sapone, *Phys. Rev. D* **74**, 123503 (2006), astro-ph/0609040.
- [58] S. Basilakos, S. Nesseris, and L. Perivolaropoulos, *Phys. Rev. D* **87**, 123529 (2013), 1302.6051.
- [59] S. Casas, V. F. Cardone, D. Sapone, N. Frusciante, F. Pace, G. Parimbelli, M. Archidiacono, K. Koyama, I. Tutusaus, S. Camera, et al., arXiv:2306.11053 (2023), 2306.11053.
- [60] Y.-S. Song and W. J. Percival, *JCAP* **10**, 004 (2009), 0807.0810.
- [61] G. Favole, B. R. Granett, J. S. Lefaurie, and D. Sapone, *Mon. Not. Roy. Astron. Soc.* **505**, 5833 (2021), 2004.13436.
- [62] A. Blanchard et al. (Euclid), *Astron. Astrophys.* **642**, A191 (2020), 1910.09273.
- [63] D. J. Eisenstein, H.-j. Seo, and M. J. White, *Astrophys. J.* **664**, 660 (2007), astro-ph/0604361.
- [64] G.-B. Zhao, L. Pogosian, A. Silvestri, and J. Zylberberg, *Phys. Rev. D* **79**, 083513 (2009), 0809.3791.
- [65] A. Hojjati, L. Pogosian, and G.-B. Zhao, *JCAP* **08**, 005 (2011), 1106.4543.
- [66] A. Zucca, L. Pogosian, A. Silvestri, and G.-B. Zhao, *JCAP* **05**, 001 (2019), 1901.05956.
- [67] Z. Wang, S. H. Mirpoorian, L. Pogosian, A. Silvestri, and G.-B. Zhao, *JCAP* **08**, 038 (2023), 2305.05667.
- [68] A. Aghamousa et al. (DESI) (2016), 1611.00036.
- [69] S. Ilić et al. (Euclid), *Astron. Astrophys.* **657**, A91 (2022), 2106.08346.
- [70] S. Nesseris and D. Sapone, *Phys. Rev. D* **92**, 023013 (2015), 1505.06601.
- [71] A. F. Agarap, arXiv preprint arXiv:1803.08375 (2018).
- [72] N. Srivastava, G. Hinton, A. Krizhevsky, I. Sutskever, and R. Salakhutdinov, *The journal of machine learning research* **15**, 1929 (2014).
- [73] X. Ying, in *Journal of physics: Conference series* (IOP Publishing, 2019), vol. 1168, p. 022022.
- [74] A. Tato and R. Nkambou (2018).
- [75] Z. Liu and F. Xu, *Frontiers in Artificial Intelligence* **6** (2023), ISSN 2624-8212, URL <https://www.frontiersin.org/articles/10.3389/frai.2023.974295>.
- [76] M. T. Ribeiro, S. Singh, and C. Guestrin, in *Proceedings of the 22nd ACM SIGKDD International Conference on Knowledge Discovery and Data Mining, San Francisco, CA, USA, August 13-17, 2016* (2016), pp. 1135–1144.
- [77] J. An, Y. Zhang, and I. Joe, *Applied Sciences* **13**, 8782 (2023).
- [78] A. T. Chantada, S. J. Landau, P. Protopapas, C. G. Scóccola, and C. Garraffo (2023), 2311.15955.
- [79] R. Srinivasan, M. Crisostomi, R. Trotta, E. Barausse, and M. Breschi (2024), 2404.12294.